Rescue of Defective Electroretinographic Responses in Dp71-Null Mice With AAV-Mediated Reexpression of Dp71

Mirella Telles Salgueiro Barboni, Cyrille Vaillend, Anneka Joachimsthaler, André Maurício Passos Liber, Hanen Khabou, Michel Roux, Ophélie Vacca, Lucile Vignaud, Deniz Dalkara, Xavier Guillonneau, et al.

Rescue of Defective Electroretinographic Responses in Dp71-Null Mice With AAV-Mediated Reexpression of Dp71

Mirella Telles Salgueiro Barboni,[1,2] Cyrille Vaillend,[3] Anneka Joachimsthaler,[4,5] André Maurício Passos Liber,[2] Hanen Khabou,[6] Michel J. Roux,[7] Ophélie Vacca,[3,6] Lucile Vignaud,[6] Deniz Dalkara,[6] Xavier Guillonneau,[6] Dora Fix Ventura,[2] Alvaro Rendon,[6] and Jan Kremers[4,5]

[1]Department of Ophthalmology, Semmelweis University, Budapest, Hungary
[2]Department of Experimental Psychology, University of São Paulo, São Paulo, Brazil
[3]Neuroscience Paris-Saclay Institute (Neuro-PSI), UMR 9197, Université Paris Sud, CNRS, Université Paris Saclay, Orsay, France
[4]Department of Ophthalmology, University Hospital Erlangen, Erlangen, Germany
[5]Department of Biology, Animal Physiology, FAU Erlangen-Nürnberg, Erlangen, Germany
[6]Department of Therapeutics, Sorbonne University, Institut de la Vision, Paris, France
[7]Department of Translational Medicine and Neurogenetics, IGBMC-ICS Phenomin, University of Strasbourg, Illkirch, France

Correspondence: Jan Kremers, University Hospital Erlangen, Schwabachanlage 6, 91054 Erlangen, Germany; jan.kremers@uk-erlangen.de.

MTSB and CV contributed equally to the paper.
AR and JK are equally responsible for the research work.

Received: August 14, 2019
Accepted: November 11, 2019
Published: February 12, 2020

Citation: Barboni MTS, Vaillend C, Joachimsthaler A, et al. Rescue of defective electroretinographic responses in Dp71-null mice with AAV-mediated reexpression of Dp71. *Invest Ophthalmol Vis Sci.* 2020;61(2):11. https://doi.org/10.1167/iovs.61.2.11

Purpose. To study the potential effect of a gene therapy, designed to rescue the expression of dystrophin Dp71 in the retinas of Dp71-null mice, on retinal physiology.

Methods. We recorded electroretinograms (ERGs) in Dp71-null and wild-type littermate mice. In dark-adapted eyes, responses to flashes of several strengths were measured. In addition, flash responses on a 25-candela/square meters background were measured. On- and Off-mediated responses to sawtooth stimuli and responses to photopic sine-wave modulation (3–30 Hz) were also recorded. After establishing the ERG phenotype, the ShH10-GFP adeno-associated virus (AAV), which has been previously shown to target specifically Müller glial cells (MGCs), was delivered intravitreously with or without (sham therapy) the Dp71 coding sequence under control of a CBA promoter. ERG recordings were repeated three months after treatment. Real-time quantitative PCR and Western blotting analyses were performed in order to quantify Dp71 expression in the retinas.

Results. Dp71-null mice displayed reduced b-waves in dark- and light-adapted flash ERGs and smaller response amplitudes to photopic rapid-on sawtooth modulation and to sine-wave stimuli. Three months after intravitreal injections of the ShH10-GFP-2A-Dp71 AAV vector, ERG responses were completely recovered in treated eyes of Dp71-null mice. The functional rescue was associated with an overexpression of Dp71 in treated retinas.

Conclusions. The present results show successful functional recovery accompanying the reexpression of Dp71. In addition, this experimental model sheds light on MGCs influencing ERG components, since previous reports showed that aquaporin 4 and Kir4.1 channels were mislocated in MGCs of Dp71-null mice, while their distribution could be normalized following intravitreal delivery of the same ShH10-GFP-2A-Dp71 vector.

Keywords: retina, Müller glial cells, electroretinogram, dystrophin, gene therapy

Dp71 is the main short product of the *DMD* gene (MIM: 300377) expressed in the central nervous system (CNS). It is generated by usage of an internal promoter located in the intron between exons 62 and 63 of the *DMD* gene.[1–4] In the rodent retina, Dp71 is selectively expressed by the Müller glial cells (MGCs) and astrocytes, at the inner limiting membrane (ILM) and around blood vessels.[5–11] It is associated with a protein complex responsible for membrane clustering and proper distribution of the aquaporin 4 (AQP4) water channel and the Kir4.1 potassium (K^+) channel in MGCs, which control extracellular water and ionic balance.[8,12]

Mutations in the multipromoter *DMD* gene, of which Dp71 is one product, have been associated with retinal alterations in both patients with Duchenne muscular dystrophy (DMD [MIM: 310200]) and mouse models of this disease.[13–24] This mostly reflects the dysfunction of *DMD* gene products affected by frequent mutations, such as Dp427 and Dp260, which are expressed in the outer plexiform layer (OPL) of the retina.[25,26] However, the most distal mutations of the *DMD* gene that additionally prevent expression of Dp71 aggravate retinal dysfunctions in patients with DMD.[22] It has also been proposed that dysfunction of the dystrophin-associated glycoprotein complex in MGCs, as well as the

mislocalization of Kir4.1 and AQP4 channels, contributes to the retinal edema and the neovascularization in diabetic retinopathy. [27–29] More recently, AQP4 disruption in patients with neuromyelitis optica has been associated with electrophysiologic alterations of the retina.[30]

MGCs constitute the main type of glial cell in the retina of the vertebrates.[31–33] In addition to other functions,[34–37] MGCs are responsible for the extracellular ionic balance of the retina,[35,38] notably by K^+ buffering, a critical cellular process associated with measurable extracellular currents controlling K^+ homeostasis.[39–43] How K^+ buffering contributes to retinal neurophysiologic functions is still unclear. Currents flowing along MGCs and synaptic activity[44–46] may mutually influence each other and thus contribute to the b-wave of the electroretinogram.[47,48] Interestingly, the genetic loss of Dp71 in Dp71-null mice impairs the polarization of Kir4.1 channels in MGCs[8,12] and induces a slight reduction of b-wave amplitudes in scotopic electroretinograms, as previously reported.[49]

Various adeno-associated virus (AAV) serotypes have proven useful in targeting retinal cells and to recover retinal deficits in mouse models of human diseases.[50–55] A recently characterized AAV vector serotype, the ShH10-GFP vector, may be of particular interest because it selectively transduces MGCs.[56,57] When injected intravitreally in Dp71-null mice, this AAV variant penetrates the retina easily, likely due to the thinner ILM in this mouse model.[57,58] To develop the first tool for Dp71 rescue strategies in the CNS, the complete murine Dp71 sequence without splicing was cloned under control of a strong ubiquitous chicken β-actin promoter for bicistronic expression of a GFP reporter gene linked to Dp71 coding sequence using the viral 2A peptide. The intravitreal injection of the ShH10-GFP-2A-Dp71 vector in Dp71-null mice was shown to induce reexpression of Dp71 in MGCs, associated with a complete relocalization and expression of AQP4 and Kir4.1 channels in MGCs, suggesting high suitability for rescue strategies in this transgenic mouse model.[57]

In the present study, we used precise in vivo electroretinographic (ERG) measurements evoked by different types of visual stimuli, which were proven to enable fine-level analyses and identification of specific cellular mechanisms and retinal cellular pathways in mice.[24] We first established that critical ERG parameters are affected in Dp71-null mice. We then demonstrated that the ERG deficits in Dp71-null mice can be recovered after intravitreal injections of the ShH10-GFP-2A-Dp71 vector, thus highlighting the role of MGCs in ERG and the potential of AAV-based gene therapy for functional recovery in retinal pathologic conditions. These data have been presented at the annual meeting of the Association for Research in Vision and Ophthalmology.[59]

Methods

Animals and Experimental Groups

Dp71-null mice were a kind gift from Prof. David Yaffe (Weizmann Institute, Rehovot, Israel). Targeted disruption of Dp71 expression in mice was generated in his laboratory by homologous recombination, by replacing most of the first and unique exon and a small part of the first intron of Dp71 by the promoter-less gene encoding a β-galneomycin resistance chimeric protein, which selectively abolished expression of Dp71 without interfering with expression of other *DMD* gene products.[61] Dp71-null mice were backcrossed for >10 generations with C57BL/6JRj mice (Janvier Labs, Le Genest-Saint-Isle, France) in CNRS-CDTA (Cryopréservation, Distribution, Typage et Archivage animal, UPS44, Orléans, France) by coauthor AR (Institut de la Vision, Paris, France). They were then transferred to the animal facility in Orsay (France) for production and maintenance of the transgenic line by crossing heterozygous females with C57BL/6JRj male mice, to generate Dp71-null and littermate control (wild-type [WT]) males for experiments. Genotype was determined by PCR analysis of tail DNA. Animals were kept under a 12-hour light-dark cycle (lights on 7:00 AM) with food and water ad libitum.

All experiments adhered to the ARVO Statement for the Use of Animals in Ophthalmic and Vision Research, and they were conducted following the guidelines of the local mouse facility (agreement D91-471-104) in compliance with European Directive 2010/63/EU and French National Committee (87/848). The experiments were approved by the animal welfare body of our institution (Institut des Neurosciences, Neuro-PSI) and Ethics Committee #59. A total of 34 male mice were tested: 22 Dp71-null mice (85.5 $\pm$ 6.8 days old) and 12 WT littermates (77.9 $\pm$ 6.8 days old). All animals first underwent ERG measurements to characterize their electrophysiologic phenotype. The mice were injected 8 to 15 days after the end of recordings: 9 mice were injected with the ShH10-GFP control AAV (sham) vector in their right eye (5 WT and 4 Dp71-null mice); 11 Dp71-null mice were injected with the ShH10-GFP-2A-Dp71 vector in their right eye. Left eyes of both WT and Dp71-null mice were used as noninjected controls (5 WT and 15 Dp71-null). In addition, the 2 eyes of 6 WT mice (i.e., total number of 12 eyes) were not injected to be used as control (total noninjected eyes from WT mice = 17). In 26 mice (15 Dp71-null and 11 WT), a second series of recordings was performed three months after injections. After the second ERG recording session, retinas were dissected out following cervical dislocation for molecular and biochemical analyses.

Animal Preparation

Prior to testing, the mice were dark-adapted at least 12 hours. All handling, preparation, and electrode placement were performed under deep red illumination to maintain dark adaptation of the retina. During the ERG recordings, the mice were positioned on a water-heated (38°C) platform, to maintain body temperature during anesthesia. The mice were anesthetized by an intramuscular injection of 25:5 mg/kg of 10% ketamine (ketamine 1000; Virbac, Carros, France)/2% xylazine (Rompun; Bayer Healthcare, Puteaux, France) in saline. A subcutaneous injection of 0.9% saline (300 µL before recordings, 100 µL after recordings) was given to prevent dehydration. Pupils were fully dilated using eye drops of 0.5% tropicamide (mydriaticum; Théa, Clermont-Ferrand, France) and 5% phenylephrine (Neosynephrine FAURE; Europhta, Monaco; one drop of each). Contact lens electrodes (Ø 3.2 mm; Mayo Corporation, Inazawa, Japan), filled with Corneregel (Dr. Mann Pharma, Berlin, Germany), were positioned on both corneas and served as active electrodes. Reference and ground needle electrodes were inserted subcutaneously, medial to the two ears and at the base of the tail, respectively. To prevent corneal ulcerations and eye infections, one drop of Tevemixine and one drop of N.A.C. (TVM Lab, Lempdes, France) were applied after ERG recordings.

Apparatus and Recordings

Recordings of full-field ERGs (binocularly) and stimuli presentation were controlled by the RetiPort system (Roland Consult, Brandenburg, Germany) using a Ganzfeld bowl (Q450SC). All signals were amplified 100,000 times, band-pass filtered between 1 and 300 hertz (Hz), and digitized at a rate of 512 (flash) or 2048 Hz (flicker). ERGs were measured in the order of increasing mean luminance to minimize adaptation time to the following stimulus conditions.

The following ERG recordings were performed in the given order (so that the mean retinal illuminance increased during the recordings).

Scotopic Flashes. Rod and mixed rod-cone mediated ERG responses were recorded to flashes with –3.7, –2.7, –1.7, –0.7, and 0.3 log candela (cd)·s/square meters (m^2) (white light) strengths on a dark background. The number of repeats (sweeps) decreased with increasing flash strength (12, 10, 8, 8, and 4). The interstimulus interval was progressively increased with increasing flash strength (1, 2, 5, 10, and 20 seconds), thereby maintaining a dark-adapted state. Similarly, the interval between each condition increased (from 10 to 120 seconds) as flash strength increased.

Mesopic On and Off Sawtooth. Rapid On and Off sawtooth stimuli eliciting increment (On) and decrement (Off) responses, respectively, were delivered with a mean luminance of 1 cd/m^2 (white light). The sawtooth temporal profile was presented at 4 Hz (i.e., with a period of 250 ms) and 100% temporal luminance contrast. Before recording On- and then Off-responses, the mouse was adapted to the 1-cd/m^2 mean luminance for two minutes. Signals from the first two stimulus cycles, each lasting one second (i.e., the first two seconds after stimulus onset), were discarded to avoid onset artifacts. Averages of 20 sweeps of one second each were obtained.

Photopic Flashes. In total, 0.3 log cd·s/m^2 white flashes upon a 25-cd/m^2 white background were delivered after a preadaptation period of two minutes to a 25-cd/m^2 white background. In total, 20 flashes with an interstimulus interval of one second were averaged.

Photopic Sine Wave. Sinusoidal luminance modulation (100% Michelson contrast; 60 cd/m^2 mean luminance, white light; two minutes of preadaptation) at 10 temporal frequencies from 3 to 30 Hz were measured randomly. Averages of 20 sweeps, each lasting one second, were obtained. As with the sawtooth stimuli, the first two sweeps were discarded.

Photopic On and Off Sawtooth. Rapid On and Off sawtooth stimuli (white light) for incremental and decremental responses, respectively, were delivered with a mean luminance of 60 cd/m^2. As in the mesopic condition, the temporal profile was a 250 ms period (i.e., delivered at 4 Hz) with 100% temporal luminance contrast. Signals from the first two stimulus cycles were discarded to avoid onset artifacts. Averages of 40 episodes of one second each were obtained.

ERG Signal Analysis

ERG components were analyzed offline by peak/trough, detection, baseline measurements, and Fourier analysis using self-written MATLAB routines (The Mathworks, Inc., Natick, MA, USA) and Excel spreadsheets (Microsoft Office 2010; Microsoft Corporation, Redmond, WA, USA). Figure 1A shows that in the dark-adapted flash ERG, the a-wave was defined as the difference between baseline (average of 17 ms before the flash) and the minimum within a 50-ms time window after stimulus onset, and the b-wave was the difference between the a-wave minimum and the b-wave maximum after digital isolation and removal of oscillatory potential (OPs) by a variable filter method.[60] Isolated OPs (Fig. 1B) were also obtained through the variable filter method. In the light-adapted flash ERG (Fig. 1C), only the b-wave was considered, as both the photopic a-wave and the photopic negative response were previously found to be very small.[24] Steady-state sine-wave modulation ERGs (Fig. 1D) underwent Fourier analysis to isolate their first harmonic (fundamental) amplitudes and phases. The first harmonic phase values were accepted for analysis only if the signal-to-noise ratio (SNR) was equal to or greater than two. SNR was calculated by dividing the first harmonic amplitude by the noise level, which was defined as the mean amplitude at frequencies ±1 Hz of the stimulus frequency.[61] For the sawtooth ERGs (Fig. 1E, 1F), the baseline was defined as the average of the first 5 ms of each response after the rapid luminance change. The first troughs were taken from baseline, with subsequent component amplitudes calculated as peak to trough from the preceding peak or trough.

Intravitreal Injections of ShH10 Vectors Coding GFP and GFP-2A-Dp71

Gene transfer to restore Dp71 expression in the Dp71-null mouse has been recently developed using AAV generated by directed evolution to selectively deliver the Dp71 coding sequence (without exons) to MGCs.[57,58] The production of the recombinant AAV vectors by plasmid cotransfection method was previously described.[57] Briefly, the resulting lysates were purified via iodixanol gradient ultracentrifugation[62]; 40% iodixanol fraction was concentrated and buffer exchanged using Amicon Ultra-15 Centrifugal Filter Units (Merk Millipore, Molsheim, France). Vector stocks were then tittered for DNase-resistant vector genomes by real-time PCR relative to a standard.[63] Each vector contained a self-complementary genome encoding the viral 2A peptide for bicistronic expression of GFP and Dp71 under the control of a ubiquitous CBA promoter. The GFP-2A-Dp71 cDNA was synthesized by GENEWIZ, Inc. (Leipzig, Germany) and cloned into an AAV plasmid (pTR-SB-smCBA) containing inverted terminal repeat regions for the packaging of the sequence of interest into ShH10 capsid. The vector was further modified with a single Y445F tyrosine to phenylalanine mutation for enhanced intracellular and nuclear trafficking,[64] which was introduced into the ShH10 capsid plasmid using a site-directed mutagenesis kit (QuikChange Lightning; Agilent Technologies, Les Ulis, France).

Vector administration was performed under deep isoflurane anesthesia (induction 4%; flow rate 1 L/min in air). The pupils of the mice were dilated by ocular instillation of phenylephrine (neosynephrine 5%; Faure Europhta, Monaco) and 0.5% tropicamide (mydriaticum; Théa) eye drops. An ultrafine 30-gauge disposable needle was passed through the sclera, at the equator and next to the limbus, into the vitreous cavity. Injection of 1 µL stock containing 1×10^{14} particles/mL of ShH10-GFP-2A-Dp71 vector or 1×10^{13} particles/mL of ShH10-GFP control vector was made with direct observation of the needle in the center of the vitreous cavity using contact lens electrodes (Mayo Corporation) filled with Corneregel (Dr. Mann Pharma, Berlin, Germany) under a Leica S6E stereomicroscope (zoom 6.3:1, 6.3×–40×;

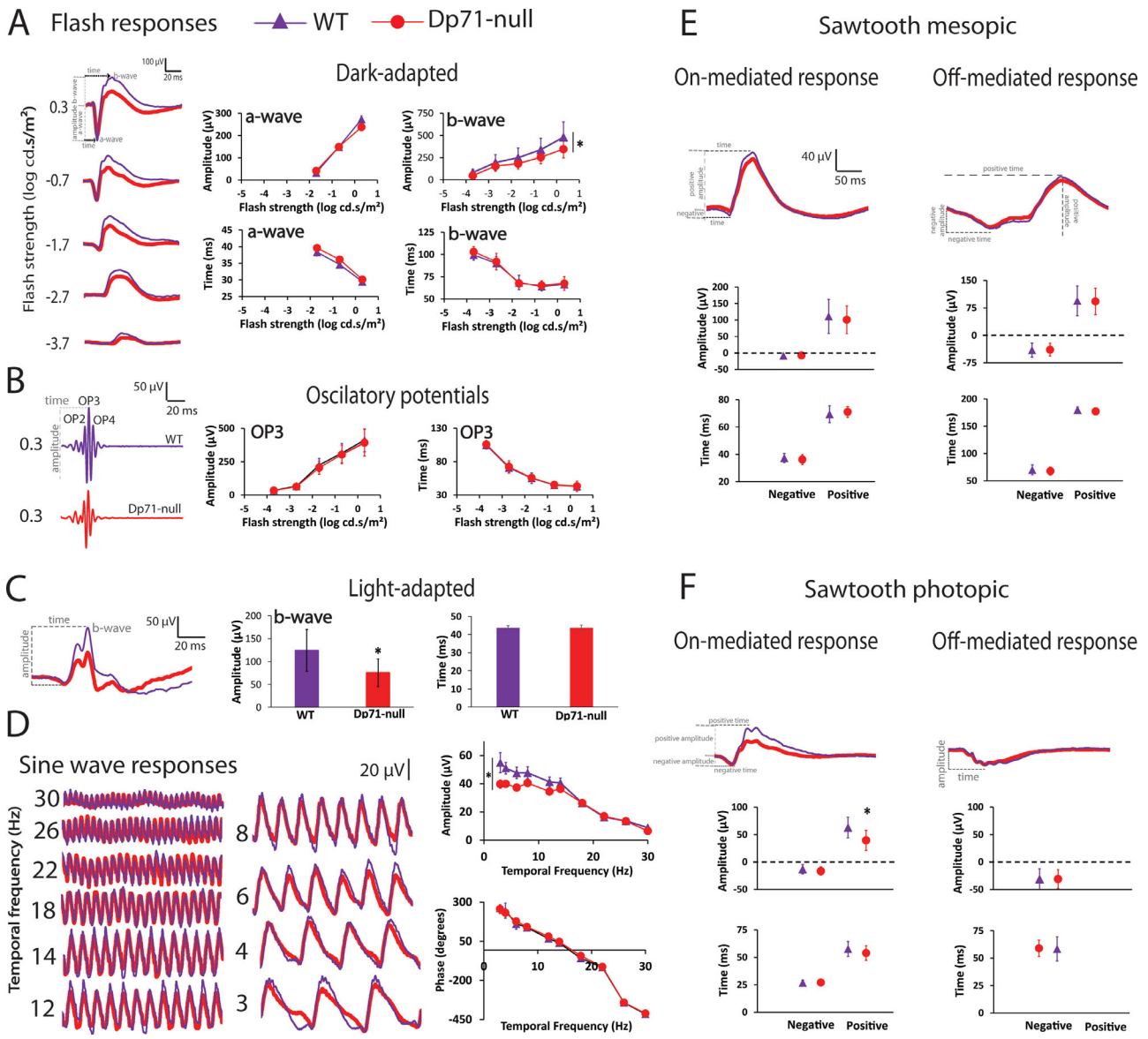

Figure 1. Averaged dark-adapted flash ERGs with OPs removed (scotopic; **A**), oscillatory potential (scotopic OP; **B**), light-adapted flash ERGs (photopic; **C**), sine-wave responses (**D**), mesopic On- and Off-mediated responses (**E**), and photopic On- and Off-mediated responses (**F**) in WT (*thin purple traces*) and Dp71-null mice (*thick red traces*). Flash strength and definitions of key components (a-wave, b-wave, isolated scotopic OPs) are indicated (see also the Methods section). OPs shown in **B** were isolated from the strongest flash response (0.3 log cd·s/m^2). Plots in **A** and **B** show the mean (± standard deviation) amplitudes (μV) and implicit times (ms) of a-wave (**A**), b-wave (**A**) and scotopic OP3 (**B**), as a function of flash strength in WT (*purple triangles*) and Dp71-null mice (*red circles*). Histograms in **C** show amplitude and implicit time of the photopic b-wave. In **D**, the plots on the right show the mean (± standard deviation) amplitudes (μV) and phases (degrees) of the first harmonic (fundamental) component as a function of temporal frequency in WT (*purple triangles*) and Dp71-null mice (*red circles*). Plots in **E** and **F** show the mean (± standard deviation) amplitudes (μV) and implicit times (ms) for the negative and positive components (as indicated) for the mesopic (**E**) and the photopic (**F**) sawtooth protocols. Significant ($P < 0.05$) genotype differences are marked with an *asterisk*.

Leica Microsystems SAS, Nanterre, France). Only right eyes were injected, whereas left eyes were used as noninjected controls.

Molecular and Biochemical Analyses

Real-Time Quantitative PCR. Total retinal RNA was extracted using the NucleoSpin RNA kit (Macherey-Nagel, Düren, Germany) and reverse transcription was performed using the QuantiTect Rev. Transcription Kit (Qiagen, Hilden, Germany) according to the manufacturer's instructions. PCR amplification of the Dp71 and GFP cDNA was performed using Master plus SYBR Green I (Roche Diagnostics, Risch-Rotkreuz, Switzerland) on a LightCycler instrument (Roche Products, Basel, Switzerland). PCR primers were designed using Primer3 software. For relative comparison, the Ct values of real-time PCR results were analyzed using the ΔCt method. The amount of cDNA was normalized to the standard internal control obtained using primers for β-actin. Primers sequences are available on request.

Western Blot Analysis. Retina samples from mice were homogenized in 250 μL RIPA Buffer (R0278; Sigma-Aldrich, St. Louis, MO, USA). Protein concentrations were

determined using bovine serum albumin (BSA) as standard. Protein extracts (25 µg) were resolved using NUPAGE 4-12% BT gels 1.0MM12W (NP0322BO; Thermofischer Scientifics, Courtaboeuf Cedex, Villebon-sur-Yvette, France) and electrotransferred using Trans-Blot Turbo Transfer Pack 0.2-µm Nitrocellulose Midi membranes (Bio-Rad Laboratories, Hercules, CA, USA) according to the manufacturer's instructions. The efficiency of protein transfer was controlled by Ponceau red staining of the blot. For immunochemistry, the membranes were blocked in PBS containing 0.1% Tween 20 (PBS-T) and 5% dry milk (Bio-Rad Laboratories) for two hours at room temperature, then incubated with the H4 polyclonal primary antibody directed against the C-terminal part of dystrophins (D. Mornet, INSERM, Montpellier, France) as described[65] in PBS-T and 5% BSA. Blots were then washed and incubated with a secondary antibody conjugated to horseradish peroxidase (Jackson Immunoresearch, Europe Ltd, Cambridgeshire, UK) diluted 1:10,000 in PBS-T, 5% BSA. Molecular weights were compared to pageruler plus prestained protein ladder (Thermo Fisher Scientific, Courtaboeuf Cedex, Villebon-sur-Yvette, France). Chemiluminescence was performed using ECL+ Western blotting detection system (Amersham Biosciences Europe GmbH, Saclay, France) and documented with a Fusion FX camera (Vilber Lourmat, Collégien, France).

Statistical Analysis

ERG data are expressed as means ± one standard deviation. Genotype and group differences were evaluated using 1- or 2-way ANOVA tests (SPSS, Statistical Package for the Social Sciences, Hong Kong, China) depending on the presence of a within-subject repeated measure (strength, frequency); paired comparisons were performed using Bonferroni post hoc analyses. Significant correlations among variables were evaluated with the r to z Fisher test; P values <0.05 were considered statistically significant.

Results

ERG Phenotype of Dp71-Null Mice

In order to describe the ERG phenotype of Dp71-null mice, we first compared ERGs from Dp71-null (N = 44 eyes; 22 males) to those from WT littermate mice (N = 24 eyes; 12 males).

The complete ERG characterization of Dp71-null mice is shown in Figure 1. Averaged dark-adapted flash responses (Fig. 1A) increased with increasing flash strength from –3.7 to 0.3 log cd·s/m^2 in Dp71-null and WT mice for both the a-wave (F(4, 256) = 484.65; P < 0.001) and the b-wave (F(4, 256) = 424.44, P < 0.001). The b-wave typically dominated the responses, while the a-wave was detectable at flash strengths of –1.7 log cd·s/m^2 and higher. Figure 1A shows comparable a-wave mean amplitudes (F(1, 64) = 0.029; P = 0.864) and implicit times (F(1, 64) = 0.287, P = 0.594) in the two genotypes. In contrast, the dark-adapted b-wave amplitudes were significantly smaller at all flash strengths in Dp71-null mice compared to WT (genotype: F(1, 64) = 14.75, P < 0.001; genotype × flash strength interaction: F(4, 256) = 9.38, P < 0.001; all post hoc analyses: P < 0.001). However, the b-wave implicit times of the dark-adapted ERGs were comparable in Dp71-null and WT mice (F(1, 64) = 0.91, P = 0.345).

Averaged isolated oscillatory potentials (Fig. 1B) were extracted from the dark-adapted responses. All OPs were extracted, but OP3 was the largest, with a maximal signal-to-noise ratio. The OP3 parameters were statistically comparable in the two genotypes (genotype effects: F(1, 66) = 1.228, P = 0.272 for amplitudes; F(1, 66) = 2.773, P = 0.101 for implicit times; genotype × strength interaction: F(4, 264) = 0.678, P = 0.608 for amplitudes; F(4, 264) = 0.842, P = 0.499 for implicit times).

In light-adapted (photopic) conditions (Fig. 1C), the ERG responses elicited by flashes of 0.3 log cd·s/m^2 strength were typically dominated by a positive b-wave. The amplitude of the photopic b-waves were also reduced (~40%) in Dp71-null compared to WT mice (F(1, 64) = 25, P < 0.001), but this was not associated with changes in the implicit times (F(1, 64) = 0.002, P < 0.961).

ERGs elicited by sine-wave luminance modulation measured at 10 temporal frequencies (3–30 Hz) are shown in Figure 1D. The mean amplitudes of the first harmonic (fundamental) components were used to define the response to sine-wave stimuli and were plotted as a function of temporal frequencies, which revealed a reduction of the first harmonic components' amplitudes at frequencies between 3 and 12 Hz in Dp71-null mice compared to WT (genotype effect: F(1, 64) = 5.268, P = 0.025; genotype × frequency effect: F(9, 576) = 4.136, P < 0.001). The phases (only from signals with SNR of two or higher; see Methods) were similar in the two groups (genotype effect: F(1, 18) = 3.772, P = 0.068; genotype × frequency effect: F(9, 162) = 0.888, P = 0.537).

Mesopic On-mediated responses had an initial small negative component followed by a larger positive component, and mesopic Off-mediated responses also displayed a negative followed by a positive component (Fig. 1E). Mean amplitudes and implicit times of negative and positive components of On-mediated mesopic responses were comparable in the two genotypes (negative component amplitude: F(1, 66) = 2.616, P = 0.111; positive component amplitude: F(1, 66) = 1.213, P = 0.275; negative component implicit time: F(1, 66) = 1.167, P = 0.284; positive component implicit time: F(1, 66) = 2.080, P = 0.154). In addition, Off-mediated mesopic responses were similar în WT and Dp71-null mice (amplitudes: F(1, 66) = 0.075, P = 0.785 and F(1, 66) = 0.016, P = 0.900; implicit times: F(1, 66) = 0.502, P = 0.481 and F(1, 66) = 1.514, P = 0.223; for the negative and positive components, respectively).

Averaged photopic On- and Off-sawtooth mediated ERG traces are shown in Figure 1F. On-responses consisted of an initial negative component with a later positive component. Off-responses contained only a negative component. There was a significant genotype-dependent amplitude difference of the positive component of the photopic On-responses (F(1, 66) = 27.25, P < 0.001) while the negative component was similar in the two genotypes (amplitude: F(1, 66) = 1.99, P = 0.162; implicit time: F(1, 66) = 0.168, P < 0.683). For photopic Off-mediated responses, amplitudes, and implicit times of the negative component were comparable in the two genotypes (negative amplitude: F(1, 66) = 0.274, P = 0.602; negative implicit time: F(1, 66) = 1.703, P = 0.196).

AAV-Mediated Rescue Experiments

After the initial characterization of phenotype differences, the same mice were used to evaluate AAV-mediated rescue

of Dp71 expression in MGCs. Their right eyes were injected with either ShH10-GFP-2A-Dp71 or ShH10-GFP (sham vector), whereas their left eyes were not injected and served as control eyes. Six WT mice were not injected; therefore, their two eyes served as noninjected control eyes.

ERG responses in untreated Dp71-null eyes, recorded three months after injections in the fellow eyes, confirmed the phenotype characterized before the injections: dark-adapted flash ERGs showed similar a-wave ($P > 0.6$) but reduced b-wave amplitudes in untreated Dp71-null mice compared to WT ($P = 0.025$) without changes in implicit times; light-adapted b-wave amplitudes were also reduced ($P < 0.001$), as well as the positive component of the photopic On-responses ($P < 0.001$) and first harmonic amplitudes of sine-wave responses ($P = 0.034$).

Our descriptions of the effects of ShH10 injections are focused on the parameters originally showing significant differences between genotypes (see above), as treatments did not modify the ERG parameters that were not initially altered in Dp71-null mice.

To determine putative biases induced by GFP expression in retinas of injected eyes, we compared the noninjected eyes with those injected with the ShH10-GFP sham vector in both genotypes (Fig. 2). To summarize, there was no effect of ShH10-GFP injection in both WT (all parameters $P > 0.9$) and Dp71-null mice (all parameters $P > 0.8$). Significant group × strength and group × frequency interactions were detected for the scotopic b-wave amplitude (Fig. 2A) and sine-wave response amplitudes (Fig. 2D) ($P < 0.001$ and $P < 0.05$, respectively), which mostly reflected the main genotype differences described above. In addition, there were slight reductions in the scotopic b-wave amplitude measured in eyes of Dp71-null mice injected with the ShH10-GFP sham vector at highest flash intensities compared to responses of the noninjected eyes (see the right plot in Fig. 2A). No differences were found in light-adapted flash (Fig. 2B), sawtooth (Fig. 2C), and sine-wave responses (Fig. 2D). In any cases, the green fluorescence of GFP did not lead to enhanced ERG responses. Hence, any enhancement after reexpression of Dp71 cannot be attributed to the expression of GFP. Data from eyes injected with the sham vector were therefore pooled with those from noninjected eyes to constitute the WT and Dp71-null control groups in the analyses of the effects of ShH10-GFP-2A-Dp71. However, we have verified that identical results could be obtained if the data were compared with those of noninjected eyes only.

ShH10-GFP-2A-Dp71 injections resulted in a full recovery of ERG responses in Dp71-null mice when compared to those measured in WT mice. As shown in Figure 3A (top traces and plots), dark-adapted (scotopic) b-wave amplitudes were significantly larger in eyes from Dp71-null mice injected with ShH10-GFP-2A-Dp71 (treated eyes) as compared to control eyes (Dp71-null control = noninjected and sham-injected eyes; $P = 0.028$), and responses in treated eyes were comparable to those recorded in the WT control group (noninjected and sham-injected eyes; $P > 0.9$). Light-adapted (photopic) ERGs also fully recovered after ShH10-GFP-2A-Dp71 injection (Fig. 3A, bottom traces and plots). Treated eyes of Dp71-null mice showed significantly larger photopic b-wave amplitudes in comparison to Dp71-null control eyes ($P < 0.001$) and were not different from amplitudes recorded in WT control eyes ($P < 0.9$). Figure 3B shows the sine-wave responses (top) and the photopic On-responses elicited by sawtooth stimulation (bottom). Sine-

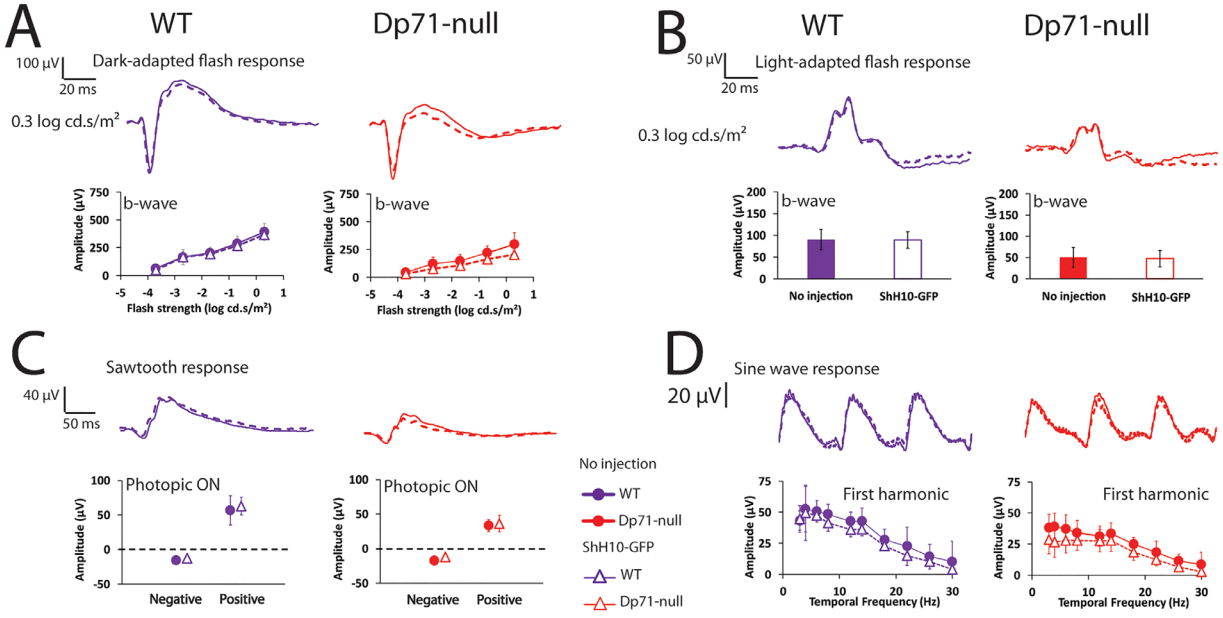

Figure 2. Effects of ShH10-GFP administration on the ERG response parameters that were found to be different between Dp71-null (*red*) and WT mice (*purple*) in the first series of recordings (as shown in Fig. 1). (**A–D**) Averaged traces are shown for eyes injected with ShH10-GFP (WT = 5 eyes and Dp71-null = 4 eyes; *dotted traces*) and noninjected eyes (WT = 17 eyes and Dp71-null = 15 eyes; *drawn traces*); plots represent means (±1 SD) in the different experimental groups as indicated (at bottom of figure, between **C** and **D**). (**A**) Responses elicited by the strongest flashes (0.3 log cd·s/m^2) in dark-adapted (scotopic) ERGs and plots of b-wave amplitudes as a function of flash strength in noninjected and ShH10-GFP-injected eyes plotted separately for Dp71-null and WT animals. (**B**) Light-adapted (photopic) flash ERG responses at 0.3 log cd·s/m and group histograms of the b-wave amplitudes. (**C**) Photopic On-responses elicited by rapid-On sawtooth stimulation and plots of the negative and positive component amplitudes. (**D**) Sine-wave responses at a temporal frequency of 3 Hz and plots of the first harmonic amplitudes as a function of temporal frequency.

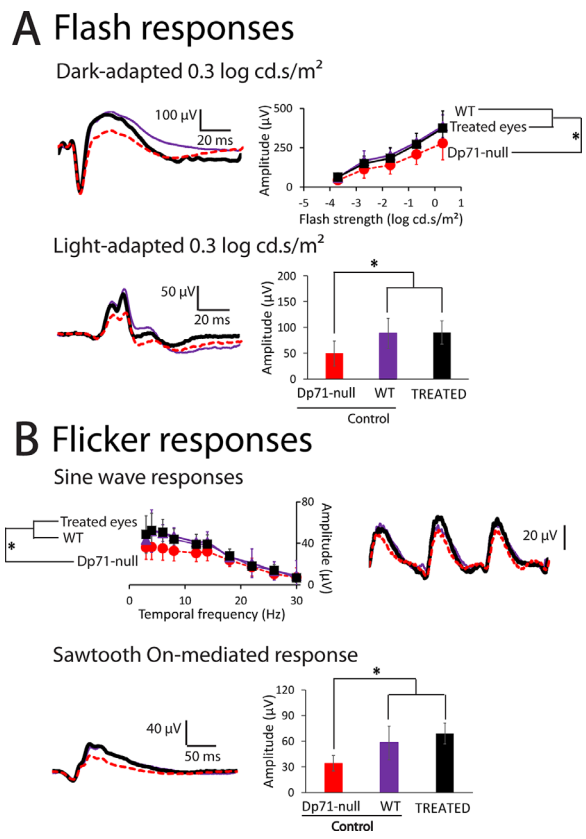

Figure 3. Effects of treatment with the ShH10-GFP-2A-Dp71 vector on dark-adapted (**A**; *top panels*) and light-adapted (**A**; *bottom panels*) flash ERGs and on flicker ERGs elicited by sine-wave modulation (**B**; *top panels*) and photopic On-sawtooth stimuli (**B**; *bottom panels*). Traces show the averaged responses recorded with the strongest flash in Dp71-null control eyes ($n = 19$; *dashed red traces*), WT control eyes ($n = 22$; *thin purple traces*), and treated eyes of Dp71-null mice ($n = 11$; *thick black traces*). In **A**, the top plot shows the mean (± standard deviation) amplitudes (µV) of the scotopic b-wave as a function of flash strength in Dp71-null controls (*red circles*), WT controls (*purple triangles*), and treated Dp71-null eyes (*black squares*), and the bottom histogram shows the mean (± standard deviation) amplitudes (µV) of the photopic b-wave in Dp71-null controls (*red bar*), WT controls (*purple bar*), and treated Dp71-null eyes (*black bar*). In **B**, the top plot shows first harmonic amplitudes (µV) of responses to sine-wave stimuli as a function of temporal frequency in Dp71-null control eyes (*red circles*), WT control eyes (*purple circles*), and treated Dp71-null eyes (*black circles*), and in the bottom plot, the histogram shows the mean (± standard deviation) amplitudes (µV) of the positive components in photopic On-responses in Dp71-null control eyes (*red bar*), WT control eyes (*purple bar*), and treated Dp71-null eyes (*black bar*). Significant ($P < 0.05$) group differences are marked with an *asterisk*.

wave response amplitudes of the treated eyes of Dp71-null mice were larger than amplitudes measured in Dp71-null control eyes ($P = 0.021$) and comparable to the amplitudes measured in WT control eyes ($P > 0.9$). The positive component of the On-responses was significantly larger in Dp71-null eyes treated with ShH10-GFP-2A-Dp71 compared to Dp71-null control eyes ($P < 0.001$). Responses recorded in treated eyes from Dp71-null mice were similar to those of WT control eyes ($P = 0.161$).

As expected from the previous characterization of our ShH10 vectors,[57] all retinas from injected eyes showed GFP expression in both quantitative PCR (qPCR) and Western blots, and Western blotting analyses revealed restoration of Dp71 expression in eyes injected with the ShH10-GFP-2A-Dp71 vector (Fig. 4). In addition, the Dp71 mRNA and protein were significantly overexpressed in the Dp71-null retinas treated with ShH10-GFP-2A-Dp71 as compared to Dp71 expression levels of WT mice. Figure 5 shows that there are no significant correlations between the level of Dp71 reexpression and posttreatment amplitudes for all affected ERG components in Dp71-null mice (all $r < 0.4$; all $P > 0.4$, NS).

Baseline Versus Posttreatment Comparison

In the foregoing, the data from control and treated Dp71-null eyes were analyzed as independent groups. However, the eyes that were treated by ShH10-GFP-2A-Dp71 injections were measured before (baseline measurement) and after (follow-up measurement) injection. This offers the possibility to directly compare the effects of treatment in the same eye, thereby evading the effects of interindividual variability in the ERG data.

During the second series of recordings (i.e., following treatment), the scotopic b-wave (Fig. 6A top) was significantly decreased in eyes from both WT ($F(1, 21) = 8.874$, $P = 0.007$) and control (noninjected and sham-injected eyes) Dp71-null mice ($F(1, 16) = 7.013$, $P = 0.018$) as compared to the recordings obtained three months before. In contrast, recordings in treated Dp71-null eyes were comparable in the two examination sessions ($F(1, 10) = 1.556$, $P = 0.241$). Similarly, photopic flash responses (Fig. 6A bottom) were lower during the follow-up session in WT ($F(1, 21) = 10.365$, $P = 0.004$) and Dp71-null control eyes ($F = 9.623$, $P = 0.006$) but not in the treated Dp71-null eyes ($F(1, 10) = 1.837$, $P = 0.205$). Hence, the dark-adapted and light-adapted b-wave amplitudes measured in the treated Dp71-null eyes were similar to those in the control WT eyes.

There was also a significant improvement in the response amplitudes to 6-Hz sine-wave stimuli (Fig. 6B, top) and to photopic sawtooth On-mediated responses (Fig. 6B, bottom) in the Dp71-null eyes after treatment (sawtooth On-responses: $F(1, 10) = 33.413$, $P < 0.001$; sine-wave responses: $F(1, 10) = 16.683$, $P = 0.002$). In contrast, no change was found between examination sessions in eyes from WT (On-responses: $F(1, 21) = 0.685$, $P = 0.417$; sine-wave responses: $F(1, 21) = 0.220$, $P = 0.644$) and noninjected Dp71-null eyes (On-responses: $F(1, 18) = 0.470$, $P = 0.502$; sine-wave responses: $F(1, 18) = 1.336$, $P = 0.263$). Again, the responses recorded from the treated injected eyes were similar to those measured in the control WT eyes.

Discussion

The main findings of the present study are as follows: (1) the absence of Dp71, the smallest product of the *DMD* gene that is normally expressed in MGCs, causes neurophysiologic disturbances in the retina characterized by ERG defects; (2) scotopic and photopic b-waves, sine-wave responses at low temporal frequencies, and photopic On-responses are altered in Dp71-null mice; and (3) reexpression of Dp71 through therapeutic intervention specifically targeting MGCs induces complete recovery of the ERG responses, showing possible perspectives for the use of gene therapy for Dp71-related diseases, such as DMD and diabetic retinopathy.

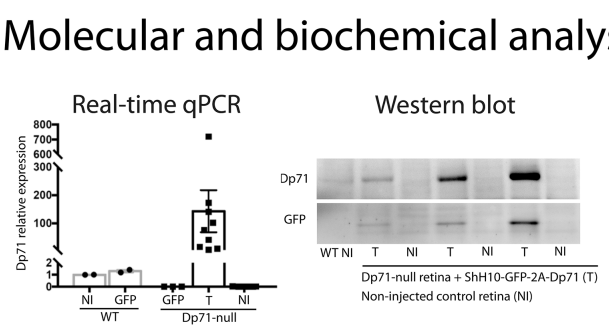

Figure 4. Overexpression of Dp71 mRNA and protein in the eyes of Dp71-null mice following intravitreal injection of the ShH10-GFP-2A-Dp71 vector. The expression level of Dp71 mRNA quantified by qPCR is shown in the left plot. Relative (re)expression in treated groups is a normalization representing the factor of changed expression compared with the mean expression in noninjected WT mice (WT-NI; mean expression equal to 1). This revealed an overexpression of Dp71 mRNA in treated eyes of Dp71-null mice (T) as compared to levels in noninjected WT eyes (WT-NI) and WT eyes injected with the sham vector (WT-GFP). Note the absence of Dp71 mRNA in eyes from Dp71-null mice that were either not injected (Dp71-null NI) or injected with the sham vector (Dp71-null-GFP). Examples of Western blots showing overexpression of the protein in treated eyes of Dp71-null mice (T) and absence of Dp71 in their respective noninjected control eyes (NI). Note the presence of GFP expression in all treated eyes.

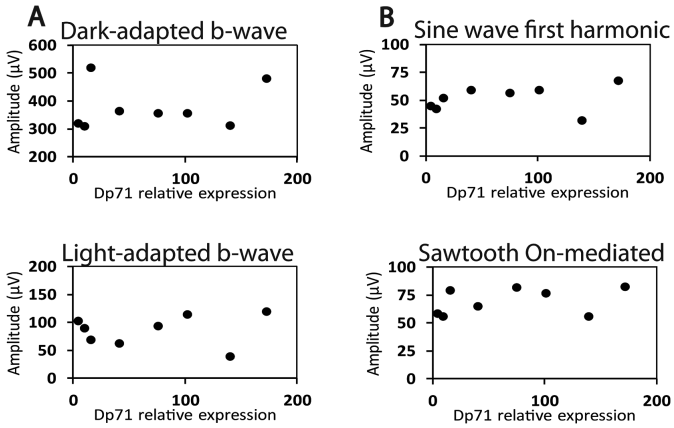

Figure 5. Correlation between Dp71 quantification and posttreatment ERG amplitudes from eight eyes of Dp71-null mice injected with the ShH10-GFP-2A-Dp71 vector. Dp71 relative expression is a normalization representing the factor of changed expression compared with the mean expression in noninjected WT mice (equal to 1), as in Figure 4. (**A**; *upper plot*) Dark-adapted b-wave amplitude at 0.3 flash strength ($r = 0.15$, $P = 0.7$) and (**A**; *lower plot*) light-adapted b-wave amplitude at 0.3 flash strength ($r = 0.10$, $P = 0.8$). (**B**; *upper plot*) Sine-wave response at 6 Hz ($r = 0.26$, $P = 0.5$) and (**B**; *lower plot*) photopic ON sawtooth response ($r = 0.34$, $P = 0.4$).

Since recovery was not directly dependent on the level of Dp71 reexpression, this approach holds even greater promise for translational developments.

The ERG is a sensitive functional biomarker of dystrophin-related alterations in the retina and possibly a signature of brain alterations. However, the specific contribution of each type of dystrophin protein expressed by retinal cells, such as Dp71, to the ERG is not well understood. Here, we applied a large repertoire of stimuli selected to achieve a detailed assessment of retinal function comparable to the one obtained previously in mdx^{3Cv}mice lacking all dystrophins[24] and to the clinical assessments performed in children with DMD.[13] Our approach confirmed the results of an earlier study[49] showing that dark-adapted (scotopic) b-waves were reduced in Dp71-null mice but also revealed alterations in other ERG parameters that enable a better understanding of the underlying retinal mechanisms in this model.

The dark-adapted ERG is normally characterized by an initial negative a-wave, mainly representing the hyperpolarization of photoreceptors and Off-bipolar cells, followed by a large positive b-wave representing On-bipolar cell activity.[44,66–70] Normal dark-adapted a-waves associated with reduced b-waves, with no peak delays and preserved OP wavelets, as found here in Dp71-null mice, indicate that On-bipolar cell postreceptoral mechanisms are specifically affected. Photopic b-waves originating from cone-driven On-bipolar cells activity were also reduced in Dp71-null mice. Moreover, the asymmetry of responses to onset versus offset photopic sawtooth stimuli suggests a selective defect in the cone On-bipolar cell pathway. Postreceptoral defects were confirmed by the presence of reduced responses to low-frequency sine-wave modulation, indicating that MGCs may play a role in sustained rather than in transient retinal pathways.

The pathogenesis induced by Dp71 loss in the mouse retina, the selective expression of Dp71 in glial cells, the specificity of our AAV-ShH10 vector targeting MGCs, and the rescued expression and subcellular localization of Dp71, AQP4, and Kir4.1 in MGCs following treatment have been characterized in detail and published previously.[8,57,58] On the basis of the previous data, we propose the following

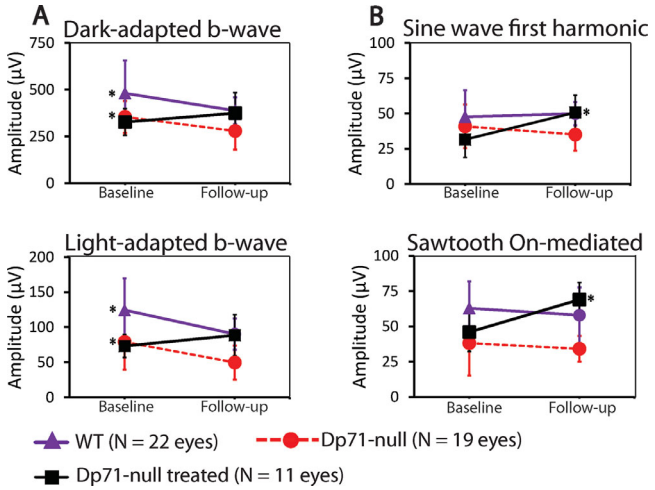

Figure 6. Response amplitudes of four ERG components previously found to be altered in Dp71-null mice measured before (baseline) and three months after (follow-up) injections. The scotopic b-wave amplitude elicited by the strongest flashes (**A**; *top panel*) and the photopic b-wave amplitude (**A**; *bottom panel*) were significantly ($P < 0.05$) reduced during the follow-up examination in both WT (purple circles) and Dp71-null control eyes (*red circles*), but not in Dp71-null treated eyes (*black circles*). The sine-wave responses (**B**; *top panel*) and the photopic sawtooth On-mediated responses (**B**; *bottom panel*) during the follow-up session were comparable to baseline responses in both WT (*purple triangles*) and Dp71-null noninjected eyes (*red circles*), while they were significantly improved in treated eyes from Dp71-null mice (*black squares*). *Asterisks* at the left side of the plots in **A** indicate that baseline amplitudes were significantly higher than follow-up amplitudes, while those at the right side in **B** indicate that they were significantly improved in the follow-up measurement.

mechanisms for retinal pathology and for structural rescue, which may explain the ERG data and can be the basis for future studies.

Retinal Dp71 is mainly expressed by MGCs, where it is necessary for the proper distribution of Kir4.1 and AQP4 channels.[8,12,71] Both channels are responsible for regulating ionic extracellular concentrations in the retina.[71–73] In human patients with mutations in the *KCNJ10* gene, coding for Kir4.1, the b-waves are delayed.[74] Surprisingly, the b-wave amplitude is unaffected in transgenic mice lacking Kir4.1,[75] and it is unaffected,[76] or mildly reduced,[77,78] in AQP4-null mice, suggesting putative compensatory mechanisms. AQP4 and Kir4.1 channels are mislocalized and downregulated in Dp71-null mice.[8] Considering that both channels influence proper K^+ homeostasis in the retina, indirectly (AQP4) or directly (Kir4.1), these disturbances may have a great impact on retinal function. Indeed, a proper distribution of Kir4.1 and AQP4 channels is required for extracellular K^+ buffering.[79,80] In Dp71-null mice, the abnormal distribution of these channels in MGCs, in addition to the downregulation of AQP4, causes changes in the extracellular ionic distribution along MGCs[8,12] that may likely lead to electrophysiologic defects.

On-bipolar cells rather than MGCs are thought to contribute directly to the b-wave and other ERG components.[44,75,81] In light of our present data, we propose a model to explain how the changed K^+ distribution in Dp71-null retina may modulate the activity of the On-bipolar cells through an altered synaptic transmission in the OPL (Fig. 7). First, the abnormal distribution of Kir4.1 and AQP4 (also downregulated) ion channels in MGCs of Dp71-null mice causes an increase in K^+ concentrations in the OPL following light-induced membrane depolarization and associated K^+ release to the extracellular space. Second, it has been reported that On-bipolar cells have a high expression level of another subtype of potassium channel, Kir2.4, in their dendritic tips.[82,83] This may result in a putatively higher sensitivity of the On-bipolar cell membrane potential to changes in extracellular K^+ concentration. Possibly, this leads to a depolarization of the membrane potential, a consequent decrease in excitability of On-bipolar cells, and thus a reduced ERG b-wave amplitude.[44] This might also explain why On- and Off-responses are differently affected in Dp71-null mice. In any case, the restoration of Dp71 after AAV treatment would lead to a normalization of K^+ distribution and to a recovery of the b-wave and other ERG components that at least partially originate in On-bipolar cells. To check if the alterations in MGCs are indeed responsible for the ERG changes, it might be interesting in future studies to measure electrophysiologic responses that are thought to directly originate in the MGCs, such as the slow PIII component or the scotopic threshold response.[44] The present study provides new evidence that the ERG defects in Dp71-null mice may reflect MGC-dependent unbalanced ion homeostasis, as they were fully compensated following the selective reexpression of Dp71 in MGCs using the ShH10-GFP-2A-Dp71 vector.

A previous study from our group has provided evidence for the altered distribution of Kir4.1 and AQP4 in the retina of Dp71-null mice.[8] In addition, we have previously demonstrated the following effects of the ShH10-GFP-2A-Dp71 AAV vector: (1) this vector serotype selectively transduces MGCs in the retina, (2) the AAV transduction territory encompasses the whole retina following intravitreous injection, (3) the reexpression of Dp71 following treatment with this vector is associated with its relocalization at the glial-vascular interface and with a relocalization of AQP4 and Kir4.1 in the same subcellular domains, and (4) the rescued distribution of Kir4.1 and AQP4 was obtained with an overexpression of Dp71 following treatment with this vector (data confirmed here). To confirm that the injections with the vector had the same effects as described previously, we repeated two experiments: we dissected each injected retina into two pieces for qPCR and Western blots. We found comparable reexpression levels as in our previous studies, characterized by overexpression of Dp71 in all treated retinas as compared to WT levels.[57,58] Therefore, the functional rescue as shown in the present study by the ERG recovery has been complemented with the demonstration that the amount of Dp71 reexpression was comparable to our previous study. We thus assume that recovery of other proteins associated with Dp71 and structural rescue of MGCs are responsible for the ERG recovery.

Additional factors may indirectly contribute to the altered b-wave amplitude in Dp71-null mice. For instance, Kir4.1 and AQP4 are necessary for blood-retina barrier (BRB) integrity,[84,85] and BRB breakdown was reported in Dp71-null mice.[9,12,57,86] However, although BRB breakdown might occur as one of the earliest detectable changes in eye diseases that also lead to impaired ERGs (e.g., in retinal vascular disorders such as diabetic retinopathy),[87,88] ERG changes are not necessarily associated with BRB breakdown.[89] The absence of Dp71 has also been associated with delayed retinal vascular development that may influence the number, morphology, and function of other retinal cells

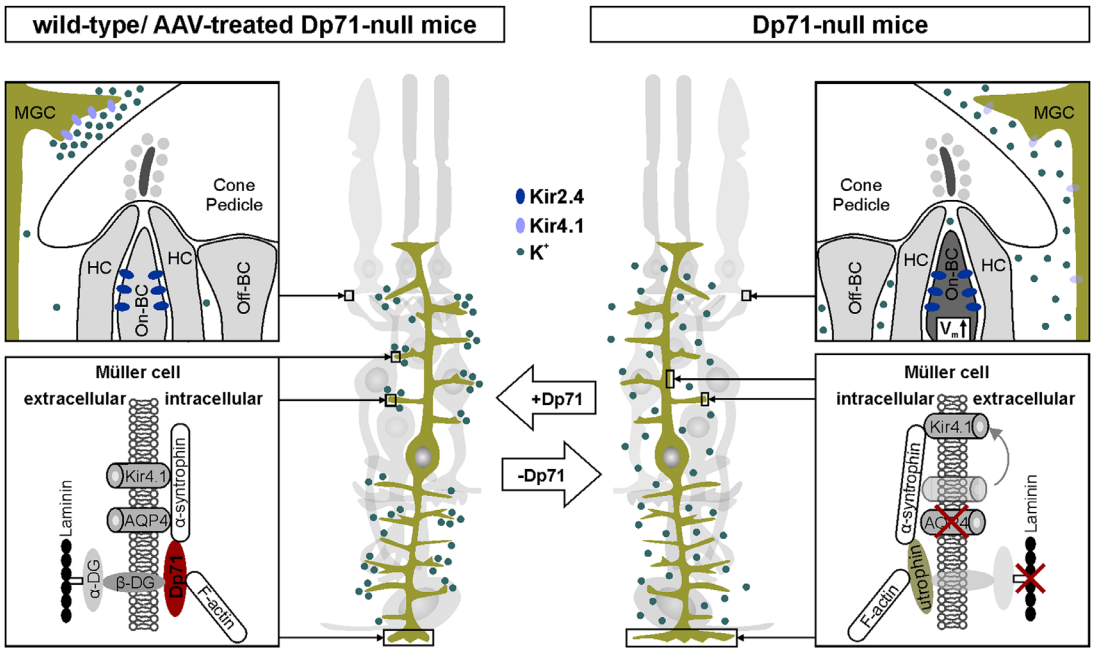

Figure 7. Illustration of a possible Dp71-dependent molecular mechanism that affects On-bipolar cell excitation and the ERGs. The large horizontal *arrows* in the middle of the illustration represent either the presence (+Dp71 pointing to the *left panel*) or the absence (–Dp71 pointing to the *right panel*) of Dp71 in wild-type/treated mice and Dp71-null mice, respectively. On the bottom-left panel, the normal (wild-type or AAV-treated Dp71-null mice) complex shows the localization of Dp71 binding α-syntrophin, which, in turn, binds the ion channels Kir4.1 and AQP4 intracellularly. Dp71 also binds β-dystroglycan (β-DG), which connects Kir4.1 and AQP4 to extracellular proteins. The proper functioning of the Dp71-dependent complex at the membrane of MGC endfeet and perivascular domains enables K^+ (*green dots*) to be distributed close to the membrane complexes, allowing ionic currents to flow. Extracellular ionic concentration ensures the proper functioning of the On-bipolar cell in the OPL (*left-top panel*). In the absence of Dp71 in Dp71-null mice (*right-bottom panel*), overexpressed utrophin replaces Dp71. The integrity of the complex is lost. This leads to an abnormal distribution of polarized AQP4 channels (*red cross*) and to a downregulation of other associated proteins such as laminin. This may lead to an increased K^+ concentration in the OPL of the Dp71-null retina (*right-top panel*). On-bipolar cells express a large number of K^+ channels possibly leading to a depolarization of the membrane potential and thus to a decreased ERG b-wave. This hypothesis was designed based on previous findings.[8,12,57,82,83]

such as the astrocytes.[9] However, it seems unlikely that the reexpression of Dp71 in MGCs of the adult retina restores developmental and/or morphologic alterations. We therefore conclude that the restoration of Kir4.1 and AQP4 clustering at MGCs in Dp71-null mice is the main mechanism to explain the ERG recovery.

Although visual symptoms in patients with DMD are not severe, the retina is possibly a sensitive biomarker for dystrophin-related CNS dysfunctions.[22] In humans, ERG disturbances are classically associated with the dystrophins normally expressed in the CNS.[13,14,17,22,23] ERG defects have also been reported in other mouse models of DMD, such as in mdx52 and mdx^{3Cv} mice.[18,19,21,24,25] However, these mouse models have alterations of several dystrophins. Therefore, possible cumulative effects may have prevented delineating the selective impact of each dystrophin on the ERG. In the present study, we characterized in detail the ERG phenotype of a mouse model that selectively lacks Dp71. Moreover, the range of stimuli used here enabled testing the integrity of distinct retinal pathways (such as photopic or scotopic, On and Off, and transient and sustained pathways). The asymmetric photopic postreceptoral disturbance found in Dp71-null mice is also a feature of ERGs obtained in patients with DMD.[13,17] Although reduced ERG b-waves have been classically attributed to the lack of Dp427 and Dp260,[15–17,19,23] our present results indicate that Dp71 loss may also cause b-wave alterations. This is in agreement with recent data from two children with DMD holding a specific deletion/mutation in exon 70 disrupting Dp71 expression and leading to electronegative scotopic ERGs.[22]

In conclusion, our results demonstrate the strong potential of gene therapies for the treatment of retinal diseases through intravitreal injection of AAV vectors. To our knowledge, we report here for the first time that neurophysiologic deficits of the retina, considered a classical nonmuscular symptom of DMD, can be successfully reversed by gene therapeutic intervention using an AAV-vector subtype designed to specifically target MGCs. This encourages the use of the ERG as a reliable noninvasive method for the rapid determination of gene therapeutic efficacy in ophthalmic conditions. ERGs may also be predictive for the success of therapeutic interventions in other parts of the CNS. Future experimental approaches that test the efficacy of DMD treatments in the CNS[90–92] may use retinal physiology, as assessed by ERGs, as a valuable biomarker. In addition, the results demonstrate that ERG components reflecting On-bipolar activity and cone pathways are influenced by Dp71-dependent MGC integrity.

Acknowledgments

The authors thank the Zootechnic platform of Neuroscience Paris-Saclay Institute for mouse breeding, care, and genotyping and Sandrine Guyon for supervision of the L2 laboratory for vector injections.

Supported by the São Paulo Research Foundation (FAPESP grant numbers 2016/22007-5 to MTSB; 2019/00777-1 to AMPL;

2016/04538-3 and 2014/26818-2 to DFV), National Council for Scientific and Technological Development (CNPq grant number 404239/2016-1 to MTSB), Agence Nationale de la Recherche (ANR, France, grant ANR-14-CE13-0037-01 to CV), Centre National de la Recherche Scientifique (CNRS, France), and University Paris-Sud (France). DFV is a CNPq 1A productivity fellow. MTSB was a fellow of Campus France (N° 931824L).

Disclosure: **M.T.S. Barboni**, None; **C. Vaillend**, None; **A. Joachimsthaler**, None; **A.M.P. Liber**, None; **H. Khabou**, None; **M.J. Roux**, None; **O. Vacca**, None; **L. Vignaud**, None; **D. Dalkara**, None; **X. Guillonneau**, None; **D.F. Ventura**, None; **A. Rendon**, None; **J. Kremers**, None

References

1. Bar S, Barnea E, Levy Z, Neuman S, Yaffe D, Nudel U. A novel product of the Duchenne muscular dystrophy gene which greatly differs from the known isoforms in its structure and tissue distribution. *Biochem J*. 1990;272:557–560.
2. Blake DJ, Love DR, Tinsley J, et al. Characterization of a 4.8kb transcript from the Duchenne muscular dystrophy locus expressed in Schwannoma cells. *Hum Mol Genet*. 1992;1:103–109.
3. Hugnot JP, Gilgenkrantz H, Vincent N, et al. Distal transcript of the dystrophin gene initiated from an alternative first exon and encoding a 75-kDa protein widely distributed in nonmuscle tissues. *Proc Natl Acad Sci USA*. 1992;89:7506–7510.
4. Rapaport D, Greenberg DS, Tal M, Yaffe D, Nudel U. Dp71, the nonmuscle product of the Duchenne muscular dystrophy gene is associated with the cell membrane. *FEBS Lett*. 1993;328:197–202.
5. Austin RC, Howard PL, D'Souza VN, Klamut HJ, Ray PN. Cloning and characterization of alternatively spliced isoforms of Dp71. *Hum Mol Genet*. 1995;4:1475–1483.
6. Claudepierre T, Dalloz C, Mornet D, Matsumura K, Sahel J, Rendon A. Characterization of the intermolecular associations of the dystrophin-associated glycoprotein complex in retinal Müller glial cells. *J Cell Sci*. 2000;113(pt 19):3409–3417.
7. Claudepierre T, Rodius F, Frasson M, et al. Differential distribution of dystrophins in rat retina. *Invest Ophthalmol Vis Sci*. 1999;40:1520–1529.
8. Dalloz C, Sarig R, Fort P, et al. Targeted inactivation of dystrophin gene product Dp71:phenotypic impact in mouse retina. *Hum Mol Genet*. 2003;12:1543–1554.
9. Giocanti-Auregan A, Vacca O, Bénard R, et al. Altered astrocyte morphology and vascular development in dystrophin-Dp71-null mice. *Glia*. 2016;64:716–729.
10. Howard PL, Dally GY, Wong MH, et al. Localization of dystrophin isoform Dp71 to the inner limiting membrane of the retina suggests a unique functional contribution of Dp71 in the retina. *Hum Mol Genet*. 1998;7:1385–1391.
11. Schmitz F, Drenckhahn D. Dystrophin in the retina. *Prog Neurobiol*. 1997;53:547–560.
12. Fort PE, Sene A, Pannicke T, et al. Kir4.1 and AQP4 associate with Dp71- and utrophin-DAPs complexes in specific and defined microdomains of Müller retinal glial cell membrane. *Glia*. 2008;56:597–610.
13. Barboni MTS, Nagy BV, de Araújo Moura AL, et al. ON and OFF electroretinography and contrast sensitivity in Duchenne muscular dystrophy. *Invest Ophthalmol Vis Sci*. 2013;54:3195–3204.
14. Barboni MTS, Martins CMG, Nagy BV, et al. Dystrophin is required for proper functioning of luminance and red-green cone opponent mechanisms in the human retina. *Invest Ophthalmol Vis Sci*. 2016;57:3581–3587.
15. Bucher F, Friedlander MS, Aguilar E, et al. The long dystrophin gene product Dp427 modulates retinal function and vascular morphology in response to age and retinal ischemia. *Neurochem Int*. 2019;129:104489.
16. Cibis GW, Fitzgerald KM, Harris DJ, Rothberg PG, Rupani M. The effects of dystrophin gene mutations on the ERG in mice and humans. *Invest Ophthalmol Vis Sci*. 1993;34:3646–3652.
17. Fitzgerald KM, Cibis GW, Giambrone SA,Harris DJ. Retinal signal transmission in Duchenne muscular dystrophy: evidence for dysfunction in the photoreceptor/depolarizing bipolar cell pathway. *J Clin Invest*. 1994;93:2425–2430.
18. Kameya S, Araki E, Katsuki M, et al. Dp260 disrupted mice revealed prolonged implicit time of the b-wave in ERG and loss of accumulation of beta-dystroglycan in the outer plexiform layer of the retina. *Hum Mol Genet*. 1997;6:2195–2203.
19. Pillers DA, Weleber RG, Green DG, et al. Effects of dystrophin isoforms on signal transduction through neural retina: genotype-phenotype analysis of duchenne muscular dystrophy mouse mutants. *Mol Genet Metab*. 1999;66:100–110.
20. Pillers DA, Fitzgerald KM, Duncan NM, et al. Duchenne/Becker muscular dystrophy: correlation of phenotype by electroretinography with sites of dystrophin mutations. *Hum Genet*. 1999;105:2–9.
21. Pillers DA, Weleber RG, Woodward WR, Green DG, Chapman VM, Ray PN. mdxCv3 mouse is a model for electroretinography of Duchenne/Becker muscular dystrophy. *Invest Ophthalmol Vis Sci*. 1995;36:462–466.
22. Ricotti V, Jägle H, Theodorou M, Moore AT, Muntoni F,Thompson DA. Ocular and neurodevelopmental features of Duchenne muscular dystrophy: a signature of dystrophin function in the central nervous system. *Eur J Hum Genet*. 2016;24:562–568.
23. Sigesmund DA, Weleber RG, Pillers DA, et al. Characterization of the ocular phenotype of Duchenne and Becker muscular dystrophy. *Ophthalmology*. 1994;101:856–865.
24. Tsai TI, Barboni MTS, Nagy BV, et al. Asymmetrical functional deficits of ON and OFF retinal processing in the mdx3Cv mouse model of Duchenne muscular dystrophy. *Invest Ophthalmol Vis Sci*. 2016;57:5788–5798.
25. D'Souza VN, Nguyen TM, Morris GE, Karges W, Pillers DA,Ray PN. A novel dystrophin isoform is required for normal retinal electrophysiology. *Hum Mol Genet*. 1995;4:837–842.
26. Wersinger E, Bordais A, Schwab Y, et al. Reevaluation of dystrophin localization in the mouse retina. *Invest Ophthalmol Vis Sci*. 2011;52:7901–7908.
27. Iandiev I, Pannicke T, Reichenbach A, Wiedemann P,Bringmann A. Diabetes alters the localization of glial aquaporins in rat retina. *Neurosci Lett*. 2007;421:132–136.
28. Reichenbach A, Wurm A, Pannicke T, Iandiev I, Wiedemann P,Bringmann A. Müller cells as players in retinal degeneration and edema. *Graefes Arch Clin Exp Ophthalmol*. 2007;245:627–636.
29. Thompson K, Chen J, Luo Q, Xiao Y, Cummins TR,Bhatwadekar AD. Advanced glycation end (AGE) product modification of laminin downregulates Kir4.1 in retinal Müller cells. *PLoS One*. 2018;13:e0193280.
30. You Y, Zhu L, Zhang T, et al. Evidence of Müller glial dysfunction in patients with aquaporin-4 immunoglobulin g-positive neuromyelitis optica spectrum disorder. *Ophthalmology*. 2019;126:801–810.
31. Boycott BB,Hopkins JM. Microglia in the retina of monkey and other mammals: its distinction from other types of glia and horizontal cells. *Neuroscience*. 1981;6:679–688.
32. Newman EA. Regional specialization of retinal glial cell membrane. *Nature*. 1984;309:155–157.

Investigative Ophthalmology & Visual Science

33. Pannicke T, Ivo Chao T, Reisenhofer M, Francke M,Reichenbach A. Comparative electrophysiology of retinal Müller glial cells: a survey on vertebrate species. *Glia*. 2017;65:533–568.
34. Edwards RB, Adler AJ, Dev S,Claycomb RC. Synthesis of retinoic acid from retinol by cultured rabbit Müller cells. *Exp Eye Res*. 1992;54:481–490.
35. Newman EA,Zahs KR. Modulation of neuronal activity by glial cells in the retina. *J Neurosci*. 1998;18:4022–4028.
36. Reichenbach A,Bringmann A. New functions of Müller cells. *Glia*. 2013;61:651–678.
37. Vecino E, Rodriguez FD, Ruzafa N, Pereiro X,Sharma SC. Glia-neuron interactions in the mammalian retina. *Prog Retin Eye Res*. 2016;51:1–40.
38. Newman EA. Membrane physiology of retinal glial (Müller) cells. *J Neurosci*. 1985;5:2225–2239.
39. Galambos R,Juhasz G. The contribution of glial cells to spontaneous and evoked potentials. *Int J Psychophysiol*. 1997;26:229–236.
40. Galambos R, Juhász G, Kékesi AK, Nyitrai G,Szilágyi N. Natural sleep modifies the rat electroretinogram. *Proc Natl Acad Sci USA*. 1994;91:5153–5157.
41. Newman EA. Inward-rectifying potassium channels in retinal glial (Müller) cells. *J Neurosci*. 1993;13:3333–3345.
42. Newman EA, Frambach DA,Odette LL. Control of extracellular potassium levels by retinal glial cell K+ siphoning. *Science*. 1984;225:1174–1175.
43. Newman EA,Odette LL. Model of electroretinogram b-wave generation: a test of the K+ hypothesis. *J Neurophysiol*. 1984;51:164–182.
44. Frishman LJ. Origins of the Electroretinogram. In: Heckenlively JR, Arden GB, ed. *Principles and Practice of Clinical Electrophysiology of Vision*. Cambridge, MA: MIT Press; 2006.
45. Rager G. The cellular origin of the b-wave in the electroretinogram: a developmental approach. *J Comp Neurol*. 1979;188:225–244.
46. Szamier RB, Ripps H, Chappell RL. Changes in ERG b-wave and Müller cell structure induced by alpha-aminoadipic acid. *Neurosci Lett*. 1981;21:307–312.
47. Miller RF, Dowling JE. Intracellular responses of the Müller (glial) cells of mudpuppy retina: their relation to b-wave of the electroretinogram. *J Neurophysiol*. 1970;33:323–341.
48. Wen R, Oakley B. K(+)-evoked Müller cell depolarization generates b-wave of electroretinogram in toad retina. *Proc Natl Acad Sci U S A*. 1990;87:2117–2121.
49. Cia D, Simonutti M, Fort PE, Doly M, Rendon A. Slight alteration of the electroretinogram in mice lacking dystrophin dp71. *Ophthalmic Res*. 2014;51:196–203.
50. Biswal MR, Han P, Zhu P, et al. Timing of antioxidant gene therapy: implications for treating dry AMD. *Invest Ophthalmol Vis Sci*. 2017;58:1237–1245.
51. Hori T, Fukutome M, Koike C. Adeno associated virus (AAV) as a tool for clinical and experimental delivery of target genes into the mammalian retina. *Biol Pharm Bull*. 2019;42:343–347.
52. Khabou H, Garita-Hernandez M, Chaffiol A, et al. Noninvasive gene delivery to foveal cones for vision restoration. *JCI Insight*. 2018;3:96029.
53. Lei B, Zhang K, Yue Y, Ghosh A, Duan D. Adeno-associated virus serotype-9 mediated retinal outer plexiform layer transduction is mainly through the photoreceptors. *Adv Exp Med Biol*. 2010;664:671–678.
54. Schön C, Sothilingam V, Mühlfriedel R, et al. Gene therapy successfully delays degeneration in a mouse model of PDE6A-linked retinitis pigmentosa (RP 43) [published online ahead of print December 7, 2017]. *Hum Gene Ther*. doi:10.1089/hum.2017.156.
55. Watanabe S, Sanuki R, Ueno S, Koyasu T, Hasegawa T, Furukawa T. Tropisms of AAV for subretinal delivery to the neonatal mouse retina and its application for in vivo rescue of developmental photoreceptor disorders. *PLoS One*. 2013;8:e54146.
56. Klimczak RR, Koerber JT, Dalkara D, Flannery JG, Schaffer DV. A novel adeno-associated viral variant for efficient and selective intravitreal transduction of rat Müller cells. *PLoS One*. 2009;4:e7467.
57. Vacca O, Charles-Messance H, El Mathari B, et al. AAV-mediated gene therapy in Dystrophin-Dp71 deficient mouse leads to blood-retinal barrier restoration and oedema reabsorption. *Hum Mol Genet*. 2016;25:3070–3079.
58. Vacca O, Darche M, Schaffer DV, et al. AAV-mediated gene delivery in Dp71-null mouse model with compromised barriers. *Glia*. 2014;62:468–476.
59. Barboni MTS, Vaillend C, Joachimsthaler A, et al. AAV-induced re-expression of Dp71 in retinal Müller glial cells recovers electroretinographic responses in Dp71-null mice. *Invest Ophthalmol Vis Sci*. 2019;60:4240–4240.
60. Harazny J, Scholz M, Buder T, Lausen B, Kremers J. Electrophysiological deficits in the retina of the DBA/2J mouse. *Doc Ophthalmol*. 2009;119:181–197.
61. Meigen T, Bach M. On the statistical significance of electrophysiological steady-state responses. *Doc Ophthalmol Adv Ophthalmol*. 1999;98:207–232.
62. Choi VW, Asokan A, Haberman RA, Samulski RJ. Production of recombinant adeno-associated viral vectors for in vitro and in vivo use. *Curr Protoc Mol Biol*. 2007; Chapter 16:Unit 16.25.
63. Aurnhammer C, Haase M, Muether N, et al. Universal real-time PCR for the detection and quantification of adeno-associated virus serotype 2-derived inverted terminal repeat sequences. *Hum Gene Ther Methods*. 2012;23:18–28.
64. Petrs-Silva H, Dinculescu A, Li Q, et al. High-efficiency transduction of the mouse retina by tyrosine-mutant AAV serotype vectors. *Mol Ther*. 2009;17:463–471.
65. Daoud F, Candelario-Martínez A, Billard J-M, et al. Role of mental retardation-associated dystrophin-gene product Dp71 in excitatory synapse organization, synaptic plasticity and behavioral functions. *PLoS One*. 2008;4:e6574.
66. Berson EL, Gouras P, Gunkel RD. Rod responses in retinitis pigmentosa, dominantly inherited. *Arch Ophthalmol*. 1968;80:58–67.
67. Brown KT. The eclectroretinogram: its components and their origins. *Vision Res*. 1968;8:633–677.
68. McCulloch DL, Marmor MF, Brigell MG, et al. ISCEV Standard for full-field clinical electroretinography (2015 update). *Doc Ophthalmol Adv Ophthalmol*. 2015;130:1–12.
69. Robson JG, Frishman LJ. Response linearity and kinetics of the cat retina: the bipolar cell component of the dark-adapted electroretinogram. *Vis Neurosci*. 1995;12:837–850.
70. Xu X, Karwoski CJ. Current source density analysis of retinal field potentials. II. Pharmacological analysis of the b-wave and M-wave. *J Neurophysiol*. 1994;72:96–105.
71. Connors NC, Kofuji P. Dystrophin Dp71 is critical for the clustered localization of potassium channels in retinal glial cells. *J Neurosci*. 2002;22:4321–4327.
72. Connors NC, Kofuji P. Potassium channel Kir4.1 macromolecular complex in retinal glial cells. *Glia*. 2006;53:124–131.
73. Kofuji P, Biedermann B, Siddharthan V, et al. Kir potassium channel subunit expression in retinal glial cells: implications for spatial potassium buffering. *Glia*. 2002;39:292–303.
74. Thompson DA, Feather S, Stanescu HC, et al. Altered electroretinograms in patients with KCNJ10 mutations and EAST syndrome. *J Physiol*. 2011;589:1681–1689.

Investigative Ophthalmology & Visual Science

75. Kofuji P, Ceelen P, Zahs KR, Surbeck LW, Lester HA, Newman EA. Genetic inactivation of an inwardly rectifying potassium channel (Kir4.1 subunit) in mice: phenotypic impact in retina. *J Neurosci*. 2000;20:5733–5740.
76. Yuan S, Zhang W, Ding J, Yao J, Jiang Q, Hu G. Increased sensitivity to retinal light damage in aquaporin-4 knockout mice. *Exp Eye Res*. 2009;89:119–122.
77. Li J, Patil RV, Verkman AS. Mildly abnormal retinal function in transgenic mice without Müller cell aquaporin-4 water channels. *Invest Ophthalmol Vis Sci*. 2002;43:573–579.
78. Da T, Verkman AS. Aquaporin-4 gene disruption in mice protects against impaired retinal function and cell death after ischemia. *Invest Ophthalmol Vis Sci*. 2004;45:4477–4483.
79. Brew H, Gray PT, Mobbs P, Attwell D. Endfeet of retinal glial cells have higher densities of ion channels that mediate K+ buffering. *Nature*. 1986;324:466–468.
80. Newman EA. Regulation of potassium levels by Müller cells in the vertebrate retina. *Can J Physiol Pharmacol*. 1987;65:1028–1032.
81. Dmitriev A, Linsenmeier RA. K+-dependent components of ERG generated by Muller cells in isolated mouse retina. *Invest Ophthalmol Vis Sci*. 2019;60:5968–5968.
82. Dhingra A, Sulaiman P, Xu Y, Fina ME, Veh RW, Vardi N. Probing neurochemical structure and function of retinal ON bipolar cells with a transgenic mouse. *J Comp Neurol*. 2008;510:484–496.
83. Sulaiman P, Xu Y, Fina ME, et al. Kir2.4 surface expression and basal current are affected by heterotrimeric G-proteins. *J Biol Chem*. 2013;288:7420–7429.
84. Nicchia GP, Pisani F, Simone L, et al. Glio-vascular modifications caused by aquaporin-4 deletion in the mouse retina. *Exp Eye Res*. 2016;146:259–268.
85. Zhang Y, Xu G, Ling Q, Da C. Expression of aquaporin 4 and Kir4.1 in diabetic rat retina: treatment with minocycline. *J Int Med Res*. 2011;39:464–479.
86. Sene A, Tadayoni R, Pannicke T, et al. Functional implication of Dp71 in osmoregulation and vascular permeability of the retina. *PLoS One*. 2009;4:e7329.
87. Cunha-Vaz J, Faria de Abreu JR, Campos AJ. Early breakdown of the blood-retinal barrier in diabetes. *Br J Ophthalmol*. 1975;59:649–656.
88. Waltman S, Krupin T, Hanish S, Oestrich C, Becker B. Alteration of the blood-retinal barrier in experimental diabetes mellitus. *Arch Ophthalmol*. 1978;96:878–879.
89. Reis A, Mateus C, Melo P, Figueira J, Cunha-Vaz J, Castelo-Branco M. Neuroretinal dysfunction with intact blood-retinal barrier and absent vasculopathy in type 1 diabetes. *Diabetes*. 2014;63:3926–3937.
90. Goyenvalle A, Griffith G, Babbs A, et al. Functional correction in mouse models of muscular dystrophy using exon-skipping tricyclo-DNA oligomers. *Nat Med*. 2015;21:270–275.
91. Relizani K, Griffith G, Echevarría L, et al. Efficacy and safety profile of tricyclo-DNA antisense oligonucleotides in Duchenne muscular dystrophy mouse model. *Mol Ther Nucleic Acids*. 2017;8:144–157.
92. Vaillend C, Perronnet C, Ros C, et al. Rescue of a dystrophin-like protein by exon skipping in vivo restores GABAA-receptor clustering in the hippocampus of the mdx mouse. *Mol Ther*. 2010;18:1683–1688.

Investigative Ophthalmology & Visual Science